

Singlet levels of the NV^- centre in diamond

L J Rogers^{1,2,3}, M W Doherty¹, M S J Barson¹, S Onoda⁴, T Ohshima⁴ and N B Manson¹

¹ Laser Physics Centre, Research School of Physics and Engineering, Australian National University, Canberra, ACT 0200, Australia

² School of Science and Mathematics, Avondale College of Higher Education, Cooranbong, NSW 2265, Australia

³ Institut für Quantenoptik, Universität Ulm, Ulm, Germany

⁴ Semiconductor Analysis and Radiation Effects Group, Japan Atomic Energy Agency, 1233 Watanuki, Takasaki, Gunma, 370-1292, Japan

E-mail: lachlan.j.rogers@quantum.diamonds

Abstract. The characteristic transition of the NV^- centre at 637 nm is between 3A_2 and 3E triplet states. There are also intermediate 1A_1 and 1E singlet states, and the infrared transition at 1042 nm between these singlets is studied here using uniaxial stress. The stress shift and splitting parameters are determined, and the physical interaction giving rise to the parameters is considered within the accepted electronic model of the centre. It is established that this interaction for the infrared transition is due to a modification of electron-electron Coulomb repulsion interaction. This is in contrast to the visible 637 nm transition where shifts and splittings arise from modification to the one-electron Coulomb interaction. It is also established that a dynamic Jahn-Teller interaction is associated with the singlet 1E state, which gives rise to a vibronic level 115 cm^{-1} above the 1E electronic state. Arguments associated with this level are used to provide experimental confirmation that the 1A_1 is the upper singlet level and 1E is the lower singlet level.

PACS numbers: 42.62.Fi, 61.72.jn, 71.70.Ej, 71.70.Fk, 78.30.-j

Keywords: nitrogen-vacancy, diamond, uniaxial stress, infrared emission, spin polarisation

Submitted to: *New Journal of Physics*

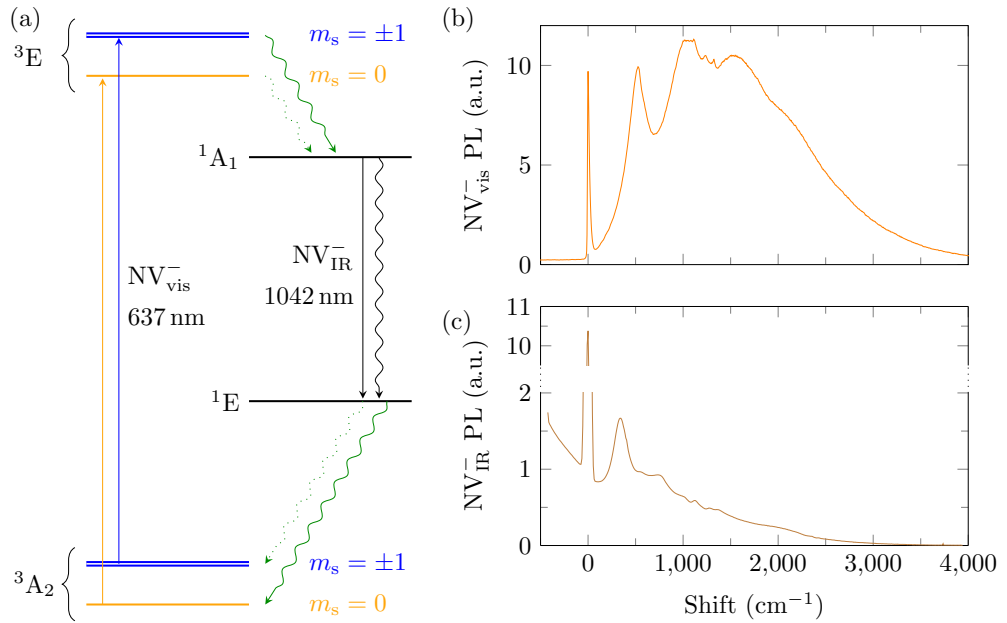


Figure 1. Electronic energy level scheme and fluorescence bands for the NV^- transitions. (a) The primary transition between triplet ground and excited states is predominantly spin conserving. Decay via the intermediate singlets gives rise to spin polarisation by preferentially switching spin from $m_s = \pm 1$ to $m_s = 0$. (b) The low temperature (10K) emission spectrum for the visible transition NV_{vis}^- . Emission was excited with 100 mW laser at 532 nm. (c) The NV_{IR}^- infrared band lies on the tail of the visible emission and has an integrated area of $1 \pm 0.2 \times 10^{-3}$ compared to that of the visible band. It is understood that the weakness of this fluorescence band is due to strongly competing non-radiative decay between the singlets illustrated by the wavy arrow in (a) [26].

1. Introduction

The negatively charged nitrogen vacancy centre in diamond (NV^-) [1] exhibits optically induced spin polarisation. This property underpins many exciting applications of the NV^- centre in fields such as magnetic sensing [2–9], biological imaging [10–12], and quantum information processing [13–17]. The principle zero-phonon line (ZPL) associated with the centre is at 637 nm (1.945 eV, 15687 cm^{-1}) and is found by uniaxial stress to involve a transition between a ground state of A symmetry and an excited state of E symmetry at a trigonal site [18]. Here we label this transition NV_{vis}^- since it is in the visible spectrum, and its fluorescence band is shown in Figure 1. The ground and excited states are spin triplets [19–23] and optical excitation of this transition results in the spin being polarised into $m_s = 0$, although this does not arise from direct optical cycling as the optical transitions are spin-conserving [24]. When the triplet system is excited there is also relaxation via intermediate singlets and this decay causes the spin polarisation. A weak emission band in the infrared (Figure 1) with a ZPL at 1042 nm (1.19 eV, 9597 cm^{-1}) is associated with decay between these two singlet levels [25].

A study of this emission (which we call NV_{IR}^-) provides an opportunity to better

understand the electronic levels in this important decay channel. Uniaxial stress is the experimental technique of choice. A previous uniaxial stress study has shown that the NV_{IR}^- transition is between levels of A and E symmetry [25], and this symmetry assignment is not in question. However, in that study the specific transitions were not correctly identified and this led to an inaccuracy of the stated stress parameters. Here the transitions are unambiguously identified and correct stress parameters are determined. In addition we experimentally resolve the long-standing contention regarding the order of the singlets [25, 27–30] and establish the 1E to be the lower singlet. The magnitudes of the stress parameters are considered within the current electronic model of the centre. It is concluded that the interaction giving rise to the shift and splitting of the infrared ZPL is different from that giving rise to the shifts and splittings of the NV_{vis}^- ZPL and NV^0 ZPL.

2. Uniaxial stress theory

The theory for uniaxial stress applied to an $A \leftrightarrow E$ transition at a site of trigonal symmetry in a cubic crystal has been given on several occasions [31–34] and has been developed by Davies and Hamer [18, 35] for the case of the NV centre. The elements of the stress tensor s_{ij} as applied to the cubic crystal can be expressed in terms of the irreducible representations appropriate for the trigonal site symmetry, and the stress perturbation at the NV site is given by

$$\begin{aligned} H^s = & \mathbf{A}_1(s_{xx} + s_{yy} + s_{zz}) + \mathbf{A}'_1(s_{yz} + s_{zx} + s_{xy}) \\ & + \mathbf{E}_X(s_{xx} + s_{yy} - 2s_{zz}) + \mathbf{E}_Y\sqrt{3}(s_{xx} - s_{yy}) \\ & + \mathbf{E}'_X(s_{yz} + s_{zx} - 2s_{xy}) + \mathbf{E}'_Y\sqrt{3}(s_{yz} - s_{zx}) \end{aligned} \quad (1)$$

where $\mathbf{A}_1, \mathbf{A}'_1$ are symmetry adapted electronic operators transforming as A_1 irreducible representations and $\mathbf{E}_X, \mathbf{E}_Y, \mathbf{E}'_X, \mathbf{E}'_Y$ are operators transforming as components of E irreducible representations [18, 33]. The stress s_{ij} is given in terms of the lattice coordinates. The effects of this interaction on an $A \leftrightarrow E$ transition have been described by Davies and Hamer [18] in terms of the following reduced matrix elements

$$A_I = \langle E | \mathbf{A}_1 | E \rangle - \langle A | \mathbf{A}_1 | A \rangle, \quad (2)$$

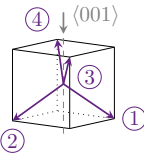
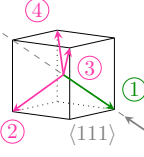
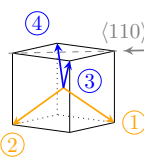
$$2A_2 = \langle E | \mathbf{A}'_1 | E \rangle - \langle A | \mathbf{A}'_1 | A \rangle, \quad (3)$$

$$\sqrt{2}B = \langle E | \mathbf{E} | E \rangle, \quad (4)$$

$$\sqrt{2}C = \langle E | \mathbf{E}' | E \rangle. \quad (5)$$

For stress applied along $\langle 001 \rangle$, $\langle 111 \rangle$ and $\langle 110 \rangle$ crystallographic directions, the resultant relative strength and polarisation of the transitions have been given in previous publications [18, 31–34] and are summarised in Table 1. Since the NV centre is now known to involve both $A_1 \leftrightarrow E$ and $A_2 \leftrightarrow E$ transitions as indicated in Figure 1 the selection rules for both cases have been included in Table 1. Stress along $\langle 001 \rangle$, $\langle 111 \rangle$ or $\langle 110 \rangle$ directions is always in a reflection plane or at right angles to a reflection plane,

Table 1. Summary of shifts, splittings and polarisation for stress applied along several crystallographic directions. The values are from reference [18] although here the values are normalised to an intensity of $8/3$ at zero stress (each of the 4 orientations contributing a relative oscillator strength of 2). Intensities are given for π (electric field vector parallel to stress) and σ (perpendicular) polarisations. The selection rules were given for $A_1 \leftrightarrow E$ transitions [18] and are extended here to also cover $A_2 \leftrightarrow E$ transitions. The change results in an interchange of X and Y and change of sign of B and C .

Stress	Orientation	Sym	E state Energy	$A_2 \leftrightarrow E$		$A_1 \leftrightarrow E$				
				π	σ	π	σ			
	①	$E_X (\Gamma_1)$	$A1 + 2B$	0	2	$\frac{8}{3}$	$\frac{2}{3}$			
	②		$54^\circ (XZ)$					$A1 - 2B$		
	③	$E_Y (\Gamma_2)$	$A1 - 2B$	$\frac{8}{3}$	$\frac{2}{3}$	0	2			
	④		$54^\circ (XZ)$					$A1 - 2B$		
	①	0°	E_X, E_Y	$A1 + 2A2$	0	1	0	1		
	②	$70^\circ (XZ)$	$E_X (\Gamma_1)$	$A1 - \frac{2}{3}A2 + \frac{4}{3}C$	0	$\frac{3}{2}$	$\frac{8}{3}$	$\frac{1}{6}$		
	③			$E_Y (\Gamma_2)$					$A1 - \frac{2}{3}A2 - \frac{4}{3}C$	
	④	$70^\circ (XZ)$	$E_Y (\Gamma_2)$	$A1 - \frac{2}{3}A2 - \frac{4}{3}C$	$\frac{8}{3}$	$\frac{1}{6}$	0	$\frac{3}{2}$		
④	$E_Y (\Gamma_2)$			$A1 - \frac{2}{3}A2 - \frac{4}{3}C$						
	①	$36^\circ (XZ)$	$E_X (\Gamma_1)$	$A1 + A2 - B + C$	0	2	0	$\frac{2}{3}$	0	$\frac{4}{3}$
	②			$E_Y (\Gamma_2)$						
	③	$90^\circ (YZ)$	$E_X (\Gamma_1)$	$A1 - A2 - B - C$	2	0	0	0	$\frac{2}{3}$	$\frac{4}{3}$
	④			$E_Y (\Gamma_2)$						
	③	$90^\circ (YZ)$	$E_X (\Gamma_1)$	$A1 - A2 - B - C$	2	0	0	0	$\frac{2}{3}$	$\frac{4}{3}$
	④			$E_Y (\Gamma_2)$						
④	$90^\circ (YZ)$	$E_Y (\Gamma_2)$	$A1 - A2 + B + C$	0	$\frac{2}{3}$	$\frac{4}{3}$	2	0	0	
④			$E_Y (\Gamma_2)$							$A1 - A2 + B + C$

and consequently the site symmetry is always lowered to C_s . Therefore, for every case the Γ_1 or Γ_2 irreducible representations for C_s are included in the table.

3. Experimental details

Diamond cubes with dimensions $2 \times 2 \times 2$ mm were used. They have nitrogen concentrations of ~ 100 ppm and were irradiated and annealed to give NV^- concentrations of ~ 5 ppm. The cubes had either $\langle 110 \rangle$, $\langle 1\bar{1}0 \rangle$ and $\langle 001 \rangle$ faces or $\langle 111 \rangle$, $\langle 1\bar{1}0 \rangle$ and $\langle 11\bar{2} \rangle$ faces. These were used for application of stress along $\langle 001 \rangle$, $\langle 111 \rangle$ and $\langle 110 \rangle$ directions by means of a pneumatic driven rod. The samples were within a cryostat and could be cooled to liquid helium or liquid nitrogen temperatures as required.

For the majority of the work the emission was excited by a laser at a wavelength of 532 nm within the vibrational sideband of the ${}^3A_2 \rightarrow {}^3E$ absorption transition. The emission at right angles was dispersed by a monochromator and detected by a photomultiplier (for NV_{vis}^-) or a cooled germanium detector (for NV_{IR}^-). A tunable dye

laser at the wavelength of the visible ZPL was used for selective excitation techniques to assist with the assignments of the NV_{IR}^- spectra.

4. Results

4.1. Uniaxial stress measurements along $\langle 001 \rangle$ and $\langle 111 \rangle$

Although both the visible [18] and infrared [25] transitions involve an $A \leftrightarrow E$ transition at a site of trigonal symmetry, NV_{vis}^- involves an A_2 state whereas NV_{IR}^- involves an A_1 . In addition, the E state is the upper level for NV_{vis}^- but for NV_{IR}^- the E is the lower level (proven later). These two differences cancel to result in the same stress patterns for the NV_{vis}^- and NV_{IR}^- transitions. Conveniently this allows the visible and infrared spectra to be easily compared to obtain the relative magnitudes of the NV_{vis}^- and NV_{IR}^- stress parameters. This is the intention of presenting Figure 2 where spectra of NV_{vis}^- and NV_{IR}^- are depicted for the same stress applied along the $\langle 001 \rangle$ and $\langle 111 \rangle$ directions.

For stress along $\langle 001 \rangle$ the splittings are the same for all orientations of the NV^- centre. The ZPL is split into two components with one component σ polarised (electric field vector perpendicular to stress) and the other predominantly π polarised (parallel to stress). The splittings are determined by the value of the B parameter (see Table 1) and the average shift is given by $A1$. It can be seen from comparing Figure 2(a) and (b) that B_{IR} is marginally larger than B_{vis} whereas $A1_{IR}$ is only about one third of $A1_{vis}$.

For $\langle 111 \rangle$ stress there are two subsets of centres (Table 1). One subset contains the centres oriented along the stress direction, for which there is no change of symmetry. This means there is no splitting, but the transition is shifted by $A1 + A2$ (Table 1). NV^- centres in this orientation are not excited when the electric field vector of the excitation is parallel to their axis, since the $A \leftrightarrow E$ transitions do not involve a z dipole moment. Consequently this orientation does not contribute to the dashed traces of Figure 2 (c) and (d) where this excitation polarisation is adopted. The NV^- centres in this orientation do give a line when transverse excitation is used. This 'extra' line is barely discernible in the case of the infrared spectrum as it overlaps the other features indicating a very small shift ($A1_{IR} + A2_{IR}$). In contrast, there is a large shift of this line for the visible transition. Since $A1_{vis}$ and $A1_{IR}$ are known from the above $\langle 001 \rangle$ stress measurements, it can be readily deduced that $A2_{vis}$ for the visible is large and negative whereas $A2_{IR}$ for the infrared is small. This information is consistent with average shifts for the centres oriented at 70° to the $\langle 111 \rangle$ stress given by $A1 + \frac{2}{3}A2$ (Table 2). The ZPL splitting for these centres depends on the C parameter, and it is apparent that C_{IR} is about one third of C_{vis} .

The conclusion that $A1_{IR}$ and C_{IR} are a factor of three smaller than their NV_{vis}^- counterparts is consistent with the NV_{IR}^- strain parameters reported previously [25]. However, there is no consistency with the $A2_{IR}$ and B_{IR} parameters. Here we have established that $A2_{IR}$ is an order of magnitude smaller than $A2_{vis}$ (instead of the factor of 2.7 given previously), and that $|B_{IR}| > |B_{vis}|$ (instead of the reverse). The previous

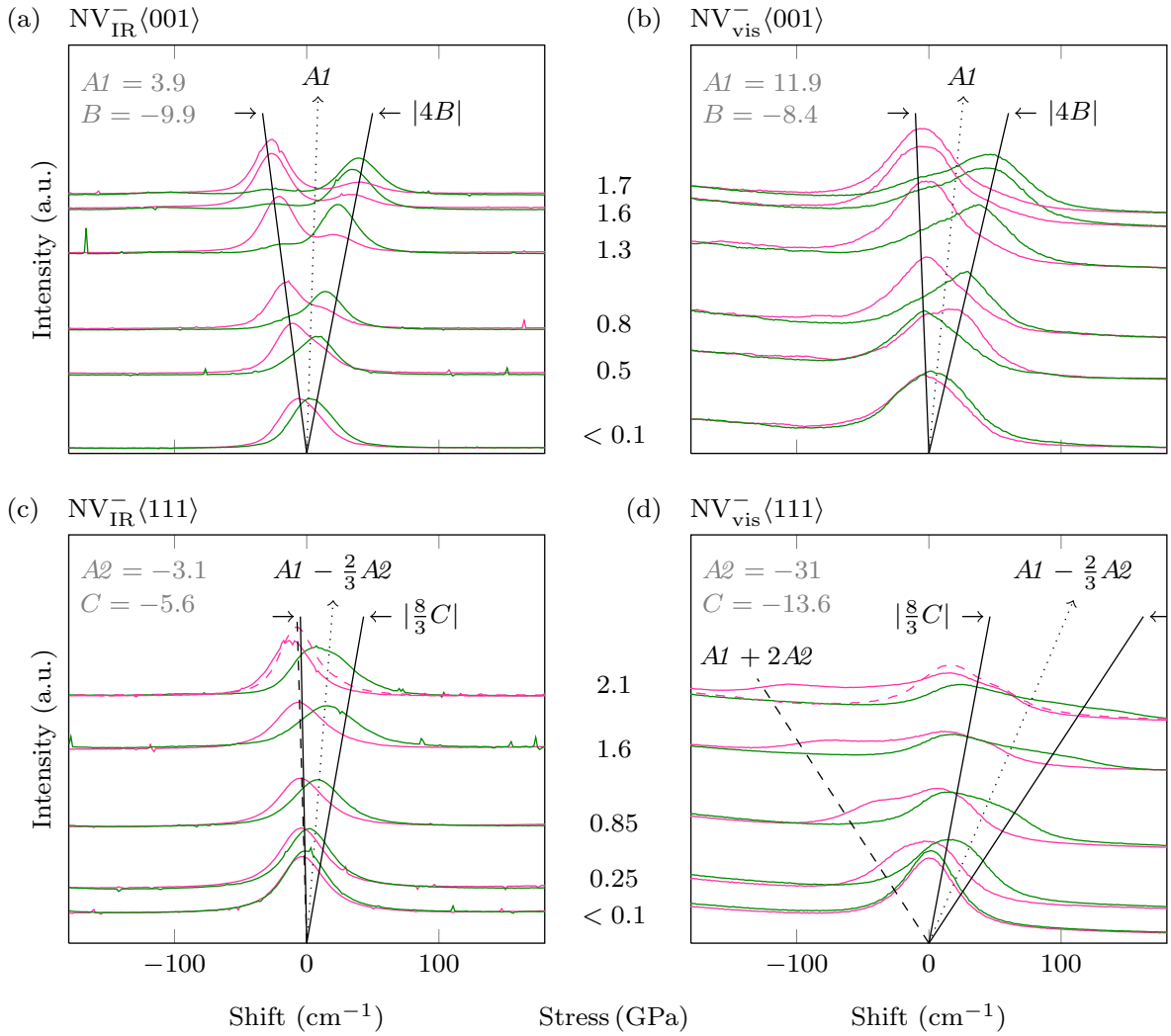


Figure 2. Uniaxial stress spectra for NV^-_{IR} on the left and NV^-_{vis} on the right. The upper traces (a) and (b) show spectra for $\langle 001 \rangle$ stress and the lower traces (c) and (d) show spectra for $\langle 111 \rangle$ stress. Excitation was from 100 mW laser at 532 nm, and emission was observed at right angles and recorded separately in π (green) and σ (magenta) polarisations. Excitation polarisation was perpendicular to the stress direction (σ) with the exception of the dashed traces in (c) and (d) where the laser polarisation was parallel to stress (π) and so the axial centres were not excited. The sample temperature was ~ 150 K. Variation of stress across the sample prevented the lines from being well resolved (and breakage prevented improvement of the data). However, identical stress settings allow the relative size of the shifts and splittings to be compared between NV^-_{IR} and NV^-_{vis} . The straight lines and annotations indicate the stress parameters calculated later (not direct fits). The NV^-_{vis} spectra are consistent with [18] and the stress parameters are those from reference [18].

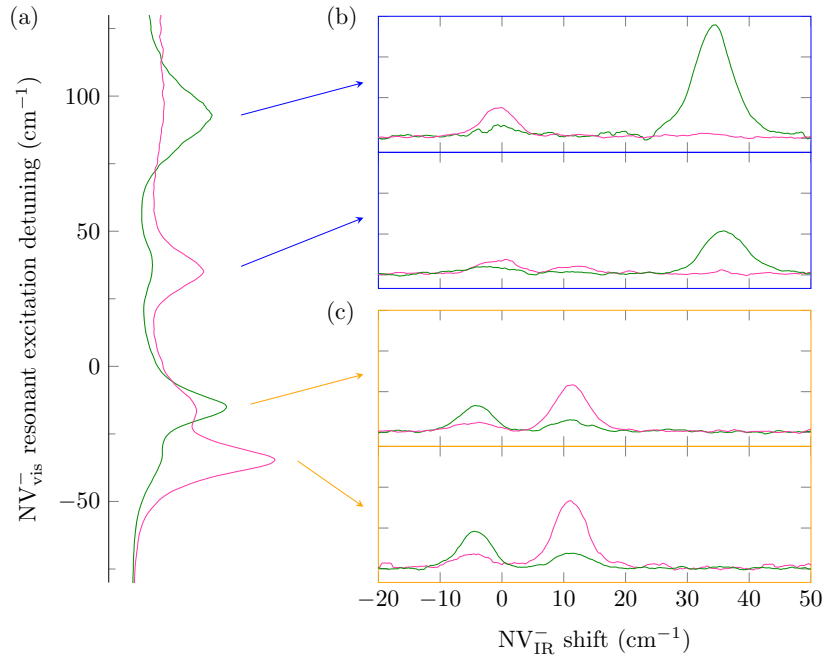


Figure 3. Uniaxial $\langle 110 \rangle$ stress spectra using resonant NV_{vis}^- excitation to assign NV_{IR}^- peaks. The exciting laser and IR detection were along $\langle 011 \rangle$, and the sample temperature was 10 K. (a) Excitation of the NV_{vis}^- transition was obtained by sweeping the excitation laser between 640 nm and 630 nm and detecting emission within the vibrational band at 700 nm. (b) IR spectra obtained with the excitation laser at fixed frequency resonant with the visible peak corresponding to the NV^- orientations ③ and ④ perpendicular to the stress (see Table 1). (c) The lower two traces framed in orange correspond to resonant excitation of orientations ① and ② at an angle of 36° to the stress.

values relied on the interpretation of spectra for stress along the $\langle 110 \rangle$ direction and, therefore, the spectra for this stress direction are re-investigated in the next section.

4.2. Uniaxial stress along $\langle 110 \rangle$ stress using selective excitation

Stress along $\langle 110 \rangle$ causes the NV^- centres to form two distinct sets of orientations, both of which have some component of transverse strain and therefore exhibit splitting (Table 1). This produces a four-line structure in the spectrum, and the determination of strain parameters depends heavily on a correct assignment of each line to a transition in a given NV orientation. Here we use selective excitation techniques to provide reliable assignments.

A 200 mW tunable dye laser was swept through the NV_{vis}^- ZPL and the emission was detected in the vibronic sideband between 650 nm and 750 nm. Weak (1 mW) 532 nm laser light was applied simultaneously to inhibit loss of signal through hole burning. The polarised NV_{vis}^- excitation spectra for a $\langle 110 \rangle$ stress of 1.4 GPa obtained in this way is shown in Figure 3(a). This NV_{vis}^- excitation spectrum is consistent with the measurements of Davies and Hamer obtained in absorption [18]. The two higher energy

lines in excitation (at 632.4 nm and 634.8 nm) are associated with centres at right angles to the stress (orientations ③ and ④, Table 1), and the lower energy NV_{vis}^- lines are associated with orientations ① and ② which are at 36° to the stress [18].

The detection filter was changed to measure emission in the NV_{IR}^- band. Resonantly exciting the two higher energy NV_{vis}^- transitions gave the polarised NV_{IR}^- spectra shown in Figure 3(b). Since these laser frequencies only excite the orientations ③ and ④ which are orthogonal to the stress, the NV_{IR}^- spectrum shows only two lines. These lines are clearly either predominantly π or σ polarised, enabling them to be assigned to the Γ_1 and Γ_2 components according to Table 1. Tuning the laser to the lower energy NV_{vis}^- transitions caused only orientations ① and ② to be excited, producing the NV_{IR}^- spectra shown in Figure 3(c). Again the lines are strongly polarised and readily assigned using Table 1. There is always the equivalence between the visible and infrared spectra described in previous section but it is noted that the order of the π and σ lines for the 36° case are reversed between the visible and infrared spectra. This results from a reversal of the relative strengths of the B and C stress parameters between the visible and infrared cases with $B_{\text{IR}} > C_{\text{IR}}$ in one case and $C_{\text{vis}} > B_{\text{vis}}$ in the other.

These selective excitation measurements provide the first unambiguous assignments of the infrared spectral features for $\langle 110 \rangle$ stress. It is now clear that the significantly different A_{IR} and B_{IR} splitting parameters given previously [25] resulted from an incorrect assignment of the NV_{IR}^- lines for $\langle 110 \rangle$ stress. In that work it was assumed that the four peaks were in the same order as for NV_{vis}^- , which does not turn out to be the case.

Having established the identity of each line in the spectrum, more conventional photoluminescence (PL) measurements were made using the 532 nm non-resonant excitation. In this way the position of the four lines in the stress spectra were followed for stress values in the range 0–3 GPa, and the shifts and splittings are shown in Figure 4. This figure also includes the results for stress along $\langle 001 \rangle$ and $\langle 111 \rangle$, where there is less ambiguity in the assignments of the lines and therefore no advantage to adopting selective excitation techniques. It can be seen from the figures that the displacements with stress are not always linear and this requires consideration before the values of the stress parameters can be deduced.

4.3. High stress and extra feature at 115 cm^{-1}

At higher stress ($> 1 \text{ GPa}$) an extra feature was found to be induced $115 \pm 5 \text{ cm}^{-1}$ to the low energy side of the ZPL and this is shown in Figure 5 for $\langle 111 \rangle$, $\langle 110 \rangle$, and $\langle 001 \rangle$ stress. The feature appears with varying intensities but increases in strength with stress at the expense of a component of the ZPL with the same polarisation. The measurements were made at higher resolution for the case of $\langle 110 \rangle$ uniaxial stress, and it is apparent that the extra feature gains at the expense of the line displaced non-linearly. It also shifts slightly in the reverse direction, as shown in Figure 4. This is typical for a situation where there are two interacting levels which have the same symmetry. From

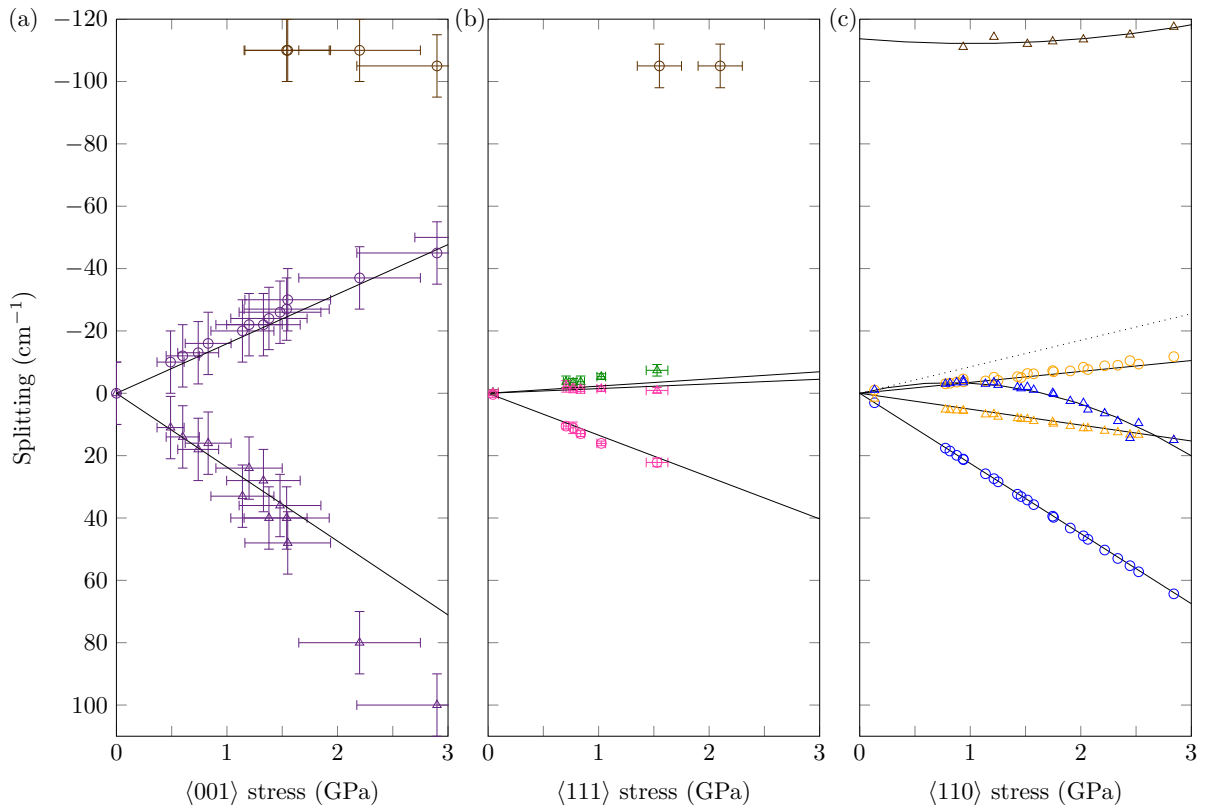


Figure 4. Strain splitting of the IR line for (a) $\langle 110 \rangle$, (b) $\langle 001 \rangle$ and (c) $\langle 111 \rangle$. The vertical scale is reversed to correspond to the emission spectrum where the lower level splits. The spectra were measured independently in π (circles) and σ (triangles) polarisation. For each stress direction the data points are coloured to match the sets of NV orientations given in Table 1. The error in stress is large in (a) due to the sample breaking over the course of the measurement.

the analysis of the ZPL it has been established that the line shifting non-linearly has Γ_1 in C_s symmetry. The extra feature will, therefore, also have Γ_1 in C_s and since it is not split it must have A_1 symmetry in C_{3v} .

This symmetry assignment is consistent with its occurrence for other stress directions. For $\langle 001 \rangle$ stress the line displaced to higher energy has π polarisation and is assigned to a Γ_1 state, and this line mixes with the extra feature (Figure 5(a)). Even though the interacting ZPL component is shifting away from the 115 cm^{-1} feature, the displacement of this ZPL line becomes non-linear as a result of the interaction, as shown in Figure 4(a). Here it might be expected that the 115 cm^{-1} feature shifts in the reverse direction, but the effect is reduced owing to the proximity of the 320 cm^{-1} vibrational level. Indeed at the highest stress it is observed that there is a slight shift of the extra feature to shorter wavelength (higher energy) owing to the latter interaction. In the third case of $\langle 111 \rangle$ the effects are small but the feature again has the same polarisation as that for the Γ_1 component of the split ZPL (Figure 5(b)).

Since the 115 cm^{-1} feature interacts with one component of a line that splits with

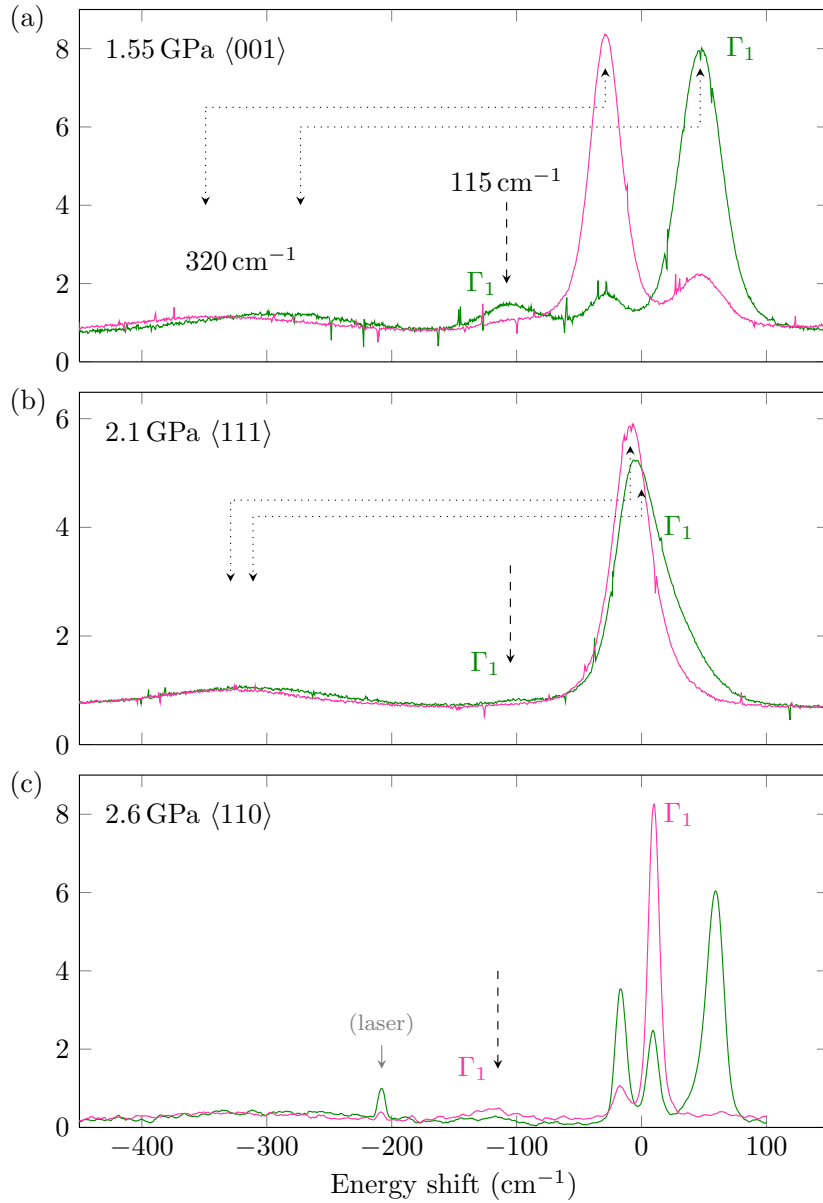


Figure 5. Uniaxial stress spectra including vibrational features. The upper trace (a) gives the spectra for $\langle 001 \rangle$ stress and the central trace (b) for $\langle 111 \rangle$ stress. In these cases the sample temperature was 150 K. (c) For $\langle 110 \rangle$ stress the sample temperature was 10 K and the higher resolution was obtained by detecting emission from a small volume using masking. In all cases the feature at 115 cm^{-1} is induced by the stress. It has the same polarisation as the Γ_1 component of the ZPL (π in the upper two traces and σ in lowest trace - see Table 1). The first vibrational sideband at 320 cm^{-1} can be seen to have the same polarisation as the ZPL indicating the vibration has A_1 symmetry.

stress, it must be associated with the 1E electronic state. It occurs on the low energy side of the ZPL in the emission spectrum. Should the 1E be the upper singlet level there will be relaxation to this level 115 cm^{-1} below the 1E state and at cryogenic temperatures ($< 30\text{ K}$) all the emission would be from this level. This is not the case and it is concluded that the 1E is not the upper singlet level. The alternative is that the 1E is the lower singlet level and the extra level lies 115 cm^{-1} above it. This confirms our previous report [36] and is consistent with the now generally accepted theoretical model [37,38].

The occurrence of low-energy vibronic levels in diamond is a fairly common observation and has been observed in previous uniaxial stress studies of diamond [35]. They are associated with a dynamic Jahn-Teller effect associated with an E state. Davies [35] has established five other cases of trigonal centres in diamond exhibiting this effect. The first vibrational state associated with a degenerate E vibration will involve the electronic and the vibration states, resulting in four vibronic states with symmetries $E \times E = A_1 + A_2 + E$. The E vibronic level is displaced up in energy and the $A_1 + A_2$ down. Quadratic electron-vibration interaction will lift the A_1 and A_2 degeneracy and result in the low lying A_1 state at 115 cm^{-1} as observed here. A similar situation arises in the case of the 2E ground state of NV^0 [35]. In this case the level occurs at 110 cm^{-1} and from the similarity in the situation it can be expected that the strength of the Jahn-Teller interaction is similar: $E_{JT}/\hbar\omega \sim 2$.

This vibronic level has significant implications. It has been used above to establish the order of the singlet levels, resolving long-standing contention about this detail of the NV electronic structure [25,27–30]. It should also be noted that one consequence of the dynamic Jahn-Teller interaction is a reduction of the effect of perturbations [39]. Thus the experimental measurements of the stress splittings will be slightly smaller than obtained from calculation unless such effects are included.

4.4. Stress parameters

The non-linear shift of some spectral features with stress is, therefore, due to interaction with vibronic levels. Modelling these interactions is not straightforward as they can involve a distribution of vibrations and the distribution need not be simple. Consequently we have determined the stress parameters using shifts and splitting at levels of stress where the strength of this latter interaction is negligible, essentially using the asymptotic slopes at zero stress. The value of the parameters are given in Table 2.

5. Discussion of the molecular model

The electronic model of the NV^- centre has its foundations in the defect-molecule approach of Coulson and Kearsley [40] and has been given in detail by many authors [1,29,37,38,41]. The centre's electronic states are written in terms of symmetry-adapted

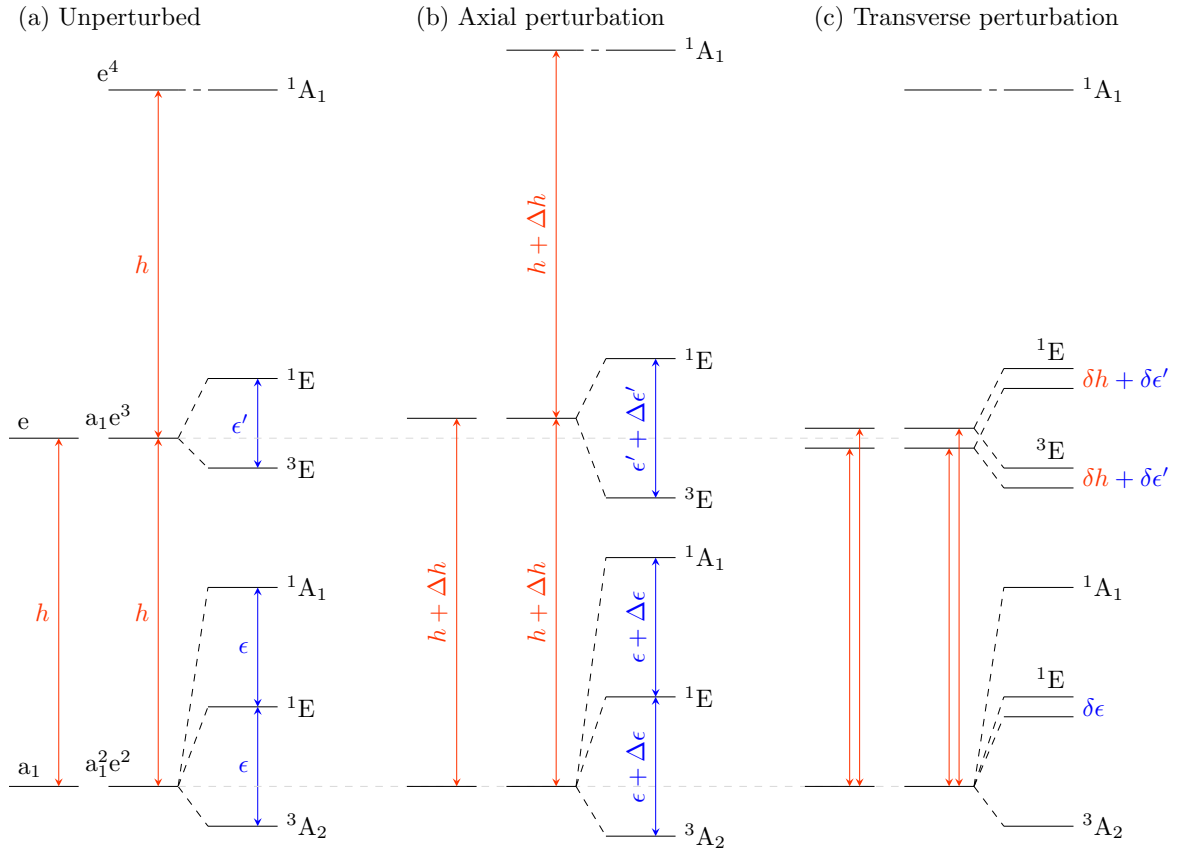


Figure 6. Electronic energy level scheme described by the molecular model for three situations. For each situation, the molecular orbital energy levels are depicted on the left, the configuration energy levels in the centre and the multi-electron state energy levels on the right. Effects arising from one-electron Coulomb interaction are coloured red, and effects arising from electron-electron interaction are blue. (a) In the unperturbed case the molecular orbitals a_1 and e are separated by energy h due to the one-electron Coulomb interaction. The three configurations associated with four electrons occupying these molecular orbitals are therefore also separated by h . The singlet and triplet energy levels within each configuration are separated by the electron-electron Coulomb repulsion interaction. In first order the three levels of the $a_1^2e^2$ configuration are equally separated by ϵ . (b) Axial strain produces a perturbed trigonal symmetry, which results in changes Δh and $\Delta\epsilon$ to the separations h and ϵ . Since trigonal symmetry is maintained, this distortion does not split the E states. (c) Transverse strain lowers the symmetry and gives rise to the splittings δh , $\delta\epsilon$ and $\delta\epsilon'$. Note in this case the only configuration that is split by the one-electron Coulomb interaction is a_1e^3 because it has an odd number of electrons occupying the e molecular orbitals. The electron-electron Coulomb repulsion interaction can split all degenerate levels. The two 1E states and the two 1A_1 states can mix through electron-electron Coulomb repulsion.

Table 2. Stress parameters of the NV^-_{IR} ZPL compared to those for NV^-_{vis} , NV^0 and N3, given in $\text{cm}^{-1}/\text{GPa}$ (meV/GPa) all $A \leftrightarrow E$ transitions at trigonal vacancy centres with adjacent nitrogen atoms. The values for NV^-_{vis} are taken from [18] although B and C sign change appropriate for $A_2 \leftrightarrow E$ transition. The values for NV^0 are from [35] and N3 from [34].

	NV^-_{IR} 1042.6 nm	NV^-_{vis} 637 nm	$NV^-_{\text{IR}}/NV^-_{\text{vis}}$ ratio	NV^0 575 nm	N3 415 nm
Param (pert)	$\text{cm}^{-1}(\text{meV})$	$\text{cm}^{-1}(\text{meV})$		$\text{cm}^{-1}(\text{meV})$	$\text{cm}^{-1}(\text{meV})$
$A1$ (A_1)	3.9 ± 0.3 (0.48)	11.9 (1.47)	0.33	8.5 (1.05)	4.0 (0.5)
$A2$ (A'_1)	-3.1 ± 0.3 (-0.38)	-31.0 (-3.85)	0.10	-28.6 (-3.55)	34 (4.2)
B (E)	-9.9 ± 0.5 (-1.23)	-8.38 (-1.04)	1.2	12.5 (1.55)	-8.5 (-1.55)
C (E')	-5.6 ± 0.5 (-0.69)	-13.6 (-1.69)	0.41	14.1 (1.76)	-11 (-1.9)

molecular orbitals. There are four unbound sp^3 atomic orbitals adjacent to the vacancy and in C_{3v} symmetry these can be linearly combined to give two degenerate orbitals that transform as the E irreducible representation (denoted as e-orbitals) and two separate orbitals of A_1 symmetry (denoted as a_1 -orbitals). These are occupied by six electrons: one from each of the adjacent carbon atoms, two from the nitrogen, and one acquired from the lattice. The lower a_1 orbital is always occupied and need not be included in a description of the states. The occupancy of the other four electrons describe the multi-electron states.

The non-relativistic electronic Hamiltonian of the NV^- centre may be defined as [37]

$$H(\vec{r}, \vec{R}) = T_e(\vec{r}) + V_{\text{Ne}}(\vec{r}, \vec{R}) + V_{\text{ee}}(\vec{r}), \quad (6)$$

where T_e is the electronic kinetic energy, V_{Ne} is the one-electron Coulomb interaction between the NV electrons and the lattice nuclei and electrons, V_{ee} is the electron-electron Coulomb repulsion interaction of the NV electrons, \vec{r} are the collective coordinates of the NV electrons and \vec{R} are the collective coordinates of the lattice. Both T_e and V_{Ne} can be written as sums of one-electron operators, whereas V_{ee} can be written as a sum of two-electron operators. The molecular orbitals are defined as solutions of the one-electron terms $T_e + V_{\text{Ne}}$. The a_1 and e molecular orbitals have energies that lie within the diamond band gap and are separated by $h \sim 2\text{eV}$ (Figure 6(a)). The energies of the a_1 and e molecular orbitals define the energies of the electronic configurations. The four electrons occupying these molecular orbitals lead to three configurations $a_1^2e^2$, a_1e^3 and e^4 , which are each separated by h (Figure 6(a)). The introduction of the electron-electron Coulomb interaction V_{ee} separates the multi-electron states within a configuration into triplet and singlet levels. The separation can be of the order of eV and, hence, comparable in magnitude to that of the one-electron terms. For example, the lowest energy configuration $a_1^2e^2$ is split into equally separated states 3A_2 , 1E and 1A_1 with separations of $\epsilon \sim 1\text{eV}$ [37, 38] (Figure 6(a)). The electron-electron Coulomb

repulsion interaction can also give interaction between configurations and mix the singlet levels of the same orbital symmetry, thereby modifying the simple expressions for ϵ and ϵ' .

The above one- and two-electron Coulomb interactions give the dominant terms in determining the effects of stress, which are observed to be several meV. Other electronic interactions such as a spin-orbit and spin-spin are less than meV and their effects are negligible compared to stress. Whilst electron-vibration interaction can be of the order of meV, it can not give stress splitting by itself. Although, as mentioned earlier, it can modify the magnitude of stress splittings in the case of dynamic Jahn-Teller interaction [39]. Hence, the analysis of the stress parameters can be largely restricted to consideration of the Coulomb interactions.

When stress is applied, the lattice coordinates \vec{R} change, which results in a change $\delta V_{Ne}[s]$ of the one-electron Coulomb interaction that in turn modifies the molecular orbitals and their energies. Furthermore, the modification of the molecular orbitals occupied by the electrons leads to a change in the electron-electron Coulomb repulsion interaction, which can be represented by the effective operator $\delta V_{ee}[s]$. Note that $\delta V_{Ne}[s] + \delta V_{ee}[s]$ can be expanded in symmetry adapted form with terms that are in one to one correlation with those in equation (1). If the symmetry is not changed by the applied stress, $\delta V_{Ne}[s]$ will only alter the a_1 -e energy separation and this is denoted by Δh (Figure 6(b)). This will result in a change of the energy separation between configurations but cause no change within each configuration (Figure 6(b)). Where the applied stress lowers the symmetry of the centre, $\delta V_{Ne}[s]$ will result in a splitting of the e molecular orbitals by δh . The consequence is that the multi-electron E states with an odd number of electrons occupying the e molecular orbitals will be split by δh (Figure 6(c)). Significantly, no splitting occurs when an even number of electrons occupy the e molecular orbitals. For each pair of electrons, one of the e electrons is moved up in energy and the other down, such that there is no overall splitting.

It is convenient to first consider the $\delta V_{Ne}[s]$ interaction in relation to the singlet transition. The ${}^1A_1(a_1^2e^2) \leftrightarrow {}^1E(a_1^2e^2)$ transition is between levels within the same $a_1^2e^2$ configuration and so the transition energy can not be shifted by $\delta V_{Ne}[s]$. In addition, the ${}^1E(a_1^2e^2)$ state has an even number of electrons occupying the e molecular orbitals and so there will be likewise no splitting arising from $\delta V_{Ne}[s]$. Mixing between singlet levels can change this situation. However, if this mixing was predominately responsible for the observed stress response of the singlet transition, the ratio of the $A1$ parameter for NV_{vis}^- and NV_{IR}^- would be same as for the $A2$ parameter. The $A1$ ratio is 0.33 and that of $A2$ is 0.1 (Table 2) and, hence, the experimental shifts of the singlet transition can not be simply explained by the $\delta V_{Ne}[s]$ interaction, even when allowing for mixing of the singlets. Likewise, the $\delta V_{Ne}[s]$ interaction with mixing would only be able to account for small splitting of ${}^1E(a_1^2e^2)$ compared to that for ${}^3E(a_1e^3)$, whereas the splitting parameters B and C for NV_{vis}^- and NV_{IR}^- are of comparable size (Table 2). The dominant interaction giving rise to the stress shift and splitting of the singlet transition at 1042 nm must result from an alternative interaction. The most

obvious candidate, given the magnitude of this interaction, is electron-electron Coulomb repulsion interaction $\delta V_{ee}[s]$. The first order changes are taken to be $\Delta\epsilon$ and $\delta\epsilon$ for axial and transverse stress, respectively (Figure 6(b) and (c)). Such perturbations can account for the change of the ${}^1A_1(a_1^2e^2)$ to ${}^1E(a_1^2e^2)$ separation and the splitting of the ${}^1E(a_1^2e^2)$ level.

The situation for the ${}^3A_2(a_1^2e^2) \leftrightarrow {}^3E(a_1e^3)$ triplet transition is very different. The transition is between states of different configuration and the ${}^3E(a_1e^3)$ state has an odd number of electrons occupying the e molecular orbitals. Consequently, the shifts and splitting of the NV_{vis}^- can arise as a consequence of the changes of the one-electron Coulomb interaction $\delta V_{Ne}[s]$. However, the possibility that there are contributions from $\delta V_{ee}[s]$ cannot immediately be eliminated. To determine how much this latter term contributes, it is worth considering the situation for NV^0 .

The NV^0 centre has one less electron and its transition is between a ${}^2E(a_1^2e)$ ground state and a ${}^2A_2(a_1e^2)$ excited state [42]. This 2E ground state has an odd number of electrons occupying the e molecular orbitals and hence can be split as a result of the $\delta V_{Ne}[s]$ interaction. It is also the sole state of the a_1^2e configuration and so there can be no contribution from $\delta V_{ee}[s]$. Therefore, the splitting of the NV^0 ZPL at 575 nm must arise solely from the $\delta V_{Ne}[s]$ interaction. The splitting is that of a single e-electron and is expected to be of similar magnitude (but opposite sign) to that of the single e-hole in the case of ${}^3E(a_1e^3)$. From Table 2 it is clear that the B and C parameters have similar magnitude for NV_{vis}^- and NV^0 , which is consistent with this expectation. This provides strong evidence that the dominant contribution to the splitting of the NV_{vis}^- transition arises from the $\delta V_{Ne}[s]$ interaction, and any contribution from $\delta V_{ee}[s]$ is minor.

The NV^- centre is the first colour centre in diamond where the stress parameters are known for two separate transitions, and this provides an ideal situation for testing theoretical calculations. For example it may help determine whether the separate contributions from one-electron Coulomb interaction and electron-electron Coulomb repulsion interaction, as outlined above, can be justified. Having similar information for a transition in the closely related neutral charge state NV^0 [35] is also valuable. The N3 centre is another nitrogen-related colour centre that has been studied by uniaxial stress [34]. It involves three nitrogen atoms and one carbon adjacent to a vacancy, rather than the three carbon and one nitrogen, and a similar molecular model is adopted for describing its electronic states. Despite the stress parameters being similar to those of NV_{vis}^- , in this case the molecular model has not successfully predicted all of the excited states [43]. Having the stress parameters for four related transitions as given in Table 2 provides valuable information for *ab initio* calculations to test our understanding of the electronic model of nitrogen-related colour centres in diamond.

6. Summary and conclusions

The aim of the work was to use uniaxial stress techniques to better understand the singlet levels of the nitrogen-vacancy centre in diamond. The 1042 nm zero-phonon

line is understood to be associated with the singlet to singlet transition between levels in the same configuration. The ZPL is spectrally narrow, the sideband is weak, and the symmetry maintaining stress shift parameters $A1$ and $A2$ are also relatively small and these are all characteristics of a transition between levels in the same electronic configuration. The ${}^1A_1(a_1^2e^2) \leftrightarrow {}^1E(a_1^2e^2)$ singlet-singlet transition is the only transition within the electronic model that satisfies this condition and these aspects all give confidence that the transition is correctly identified. However, the stress splitting parameters are large and comparable with those for the $A \leftrightarrow E$ triplet and doublet transitions of NV_{vis}^- and NV^0 , respectively. These latter transitions involve a change of configuration and an E state with an odd number of e electrons. Consequently, one-electron Coulomb interaction can account for such effects. The singlet-singlet transition is different since the one-electron Coulomb interaction can not (in first order) split or shift the ZPL, and so it was anticipated the responses would be smaller. The strain parameters for NV_{IR}^- must arise from an alternative interaction and in this work it has been shown that they can be attributed to the two-electron Coulomb repulsion term. It is recognised within the Coulson and Kearsley [40] model that Coulomb repulsion always plays a significant role and in the case of the NV^- centre this interaction is of comparable magnitude to the one-electron Coulomb term. It is, therefore, realistic that the one-electron and two-electron Coulomb interactions can result in similar energy changes in response to a distortion of the lattice. The conclusion is that there is overall consistency with the current electronic model of the NV^- and it follows that there is an adequate understanding of the singlet states.

The present uniaxial stress studies have also established that there is a dynamic Jahn-Teller effect associated with the 1E level. Combining this observation with previous reports of dynamic Jahn-Teller effect in the excited 3E state, it is clear that electron-vibration interaction is significant within the NV^- system. The presence of electron-vibration interaction has been determined from observations within the 1E and 3E degenerate electronic states independently, but the interaction can have more significant consequences between states. In particular, it can play a role in inter-system crossing between 3E and 1A_1 and between 1E and 3A_2 triplet and play a very important role in giving rise to the important spin polarisation property of NV^- .

Acknowledgements

This work was supported by the Australian Research Council (DP 120102232).

References

- [1] Marcus W. Doherty, Neil B. Manson, Paul Delaney, Fedor Jelezko, Jörg Wrachtrup, and Lloyd C.L. Hollenberg. The nitrogen-vacancy colour centre in diamond. *Physics Reports*, 528(1):1 – 45, 2013.
- [2] Boris M. Chernobrod and Gennady P. Berman. Spin microscope based on optically detected magnetic resonance. *Journal of Applied Physics*, 97(1):014903, 2005.

- [3] C. L. Degen. Scanning magnetic field microscope with a diamond single-spin sensor. *Appl. Phys. Lett.*, 92:243111, 2008.
- [4] J. M. Taylor, P. Cappellaro, L. Childress, L. Jiang, D. Budker, P. R. Hemmer, A. Yacoby, R. Walsworth, and M. D. Lukin. High-sensitivity diamond magnetometer with nanoscale resolution. *Nature Physics*, 4:810 – 816, 2008.
- [5] J. R. Maze, P. L. Stanwix, J. S. Hodges, S. Hong, J. M. Taylor, P. Cappellaro, L. Jiang, M. V. Gurudev Dutt, E. Togan, A. S. Zibrov, A. Yacoby, R. L. Walsworth, and M. D. Lukin. Nanoscale magnetic sensing with an individual electronic spin in diamond. *Nature*, 455:644 – 647, 2008.
- [6] Gopalakrishnan Balasubramanian, I. Y. Chan, Roman Kolesov, Mohannad Al-Hmoud, Julia Tisler, Chang Shin, Changdong Kim, Aleksander Wojcik, Philip R. Hemmer, Anke Krueger, Tobias Hanke, Alfred Leitenstorfer, Rudolf Bratschitsch, Fedor Jelezko, and Jörg Wrachtrup. Nanoscale imaging magnetometry with diamond spins under ambient conditions. *Nature*, 455:648 – 651, 2008.
- [7] L. T. Hall, J. H. Cole, C. D. Hill, and L. C. L. Hollenberg. Sensing of fluctuating nanoscale magnetic fields using nitrogen-vacancy centers in diamond. *Physical Review Letters*, 103(22):220802, November 2009. Copyright (C) 2010 The American Physical Society; Please report any problems to prola@aps.org.
- [8] Jared H Cole and Lloyd C L Hollenberg. Scanning quantum decoherence microscopy. *Nanotechnology*, 20(49):495401, December 2009.
- [9] Liam T Hall, Charles D Hill, Jared H Cole, and Lloyd C. L Hollenberg. Ultra-sensitive diamond magnetometry using optimal dynamic decoupling. *1003.3699*, March 2010.
- [10] Chi-Cheng Fu, Hsu-Yang Lee, Kowa Chen, Tsong-Shin Lim, Hsiao-Yun Wu, Po-Keng Lin, Pei-Kuen Wei, Pei-Hsi Tsao, Huan-Cheng Chang, and Wunshain Fann. Characterization and application of single fluorescent nanodiamonds as cellular biomarkers. *Proceedings of the National Academy of Sciences*, 104(3):727 – 732, January 2007.
- [11] Yi-Ren Chang, Hsu-Yang Lee, Kowa Chen, Chun-Chieh Chang, Dung-Sheng Tsai, Chi-Cheng Fu, Tsong-Shin Lim, Yan-Kai Tzeng, Chia-Yi Fang, Chau-Chung Han, Huan-Cheng Chang, and Wunshain Fann. Mass production and dynamic imaging of fluorescent nanodiamonds. *Nat. Nanotechnol.*, 3:284–288, 2008.
- [12] Julia Tisler, Gopalakrishnan Balasubramanian, Boris Naydenov, Roman Kolesov, Bernhard Grotz, Rolf Reuter, Jean-Paul Boudou, Patrick A. Curmi, Mohamed Sennour, Alain Thorel, Michael Börsch, Kurt Aulenbacher, Rainer Erdmann, Philip R. Hemmer, Fedor Jelezko, and Jörg Wrachtrup. Fluorescence and spin properties of defects in single digit nanodiamonds. *ACS Nano*, 3(7):1959–1965, July 2009.
- [13] Torsten Gaebel, Michael Domhan, Iulian Popa, Christoffer Wittmann, Philipp Neumann, Fedor Jelezko, James R. Rabeau, Nikolas Stavrias, Andrew D. Greentree, Steven Praver, Jan Meijer, Jason Twamley, Philip R. Hemmer, and Jorg Wrachtrup. Room-temperature coherent coupling of single spins in diamond. *Nature Physics*, 2:408, June 2006.
- [14] M. V. Gurudev Dutt, L. Childress, E. Togan L. Jiang, J. Maze, F. Jelezko, A. S. Zibrov, P. R. Hemmer, and M. D. Lukin. Quantum register based on individual electronic and nuclear spin qubits in diamond. *Science*, 316:1312–1316, June 2007.
- [15] E. Togan, Y. Chu, A. S. Trifonov, L. Jiang, J. Maze, L. Childress, M. V. G. Dutt, A. S. Sorensen, P. R. Hemmer, A. S. Zibrov, and M. D. Lukin. Quantum entanglement between an optical photon and a solid-state spin qubit. *Nature*, 466(7307):730–734, 2010.
- [16] P. Neumann, R. Kolesov, B. Naydenov, J. Beck, F. Rempp, M. Steiner, V. Jacques, G. Balasubramanian, M. L. Markham, D. J. Twitchen, S. Pezzagna, J. Meijer, J. Twamley, F. Jelezko, and J. Wrachtrup. Quantum register based on coupled electron spins in a room-temperature solid. *Nat Phys*, 6(4):249–253, April 2010.
- [17] G. D. Fuchs, V. V. Dobrovitski, R. Hanson, A. Batra, C. D. Weis, T. Schenkel, and D. D. Awschalom. Excited-state spectroscopy using single-spin manipulation in diamond. *Phys. Rev.*

- Lett.*, 101:117601, 2008.
- [18] Gordon Davies and M F Hamer. Optical studies of the 1.945 eV vibronic band in diamond. *Proc. R. Soc. Lond. A.*, 348:285–298, 1976.
 - [19] J.H.N. Loubser and J.A. Van Wyk. Optical spin-polarization in a triplet state in irradiated and annealed type 1b diamonds. *Diamond Res.*, 1:11 – 15, 1977.
 - [20] J. H. N. Loubser and J. A. van Wyk. Electron spin resonance in the study of diamond. *Reports on Progress in Physics*, 41(8):1201, August 1978.
 - [21] N. R. S. Reddy, N. B. Manson, and E. R. Krausz. Two-laser spectral hole burning in a colour centre in diamond. *J. Lumin.*, 38:46, December 1987.
 - [22] E. van Oort, N.B. Manson, and M. Glasbeek. Optically detected spin coherence of the diamond n-v centre in its triplet ground state. *J. Phys. C*, 21:4385, 1988.
 - [23] D. A Redman, S. Brown, R. H Sands, and S. C Rand. Spin dynamics and electronic states of n-v centers in diamond by EPR and four-wave-mixing spectroscopy. *Phys. Rev. Lett.*, 67(24):3420 – 3423, December 1991.
 - [24] N. B. Manson, J. P. Harrison, and M. J. Sellars. Nitrogen-vacancy center in diamond: Model of the electronic structure and associated dynamics. *Phys. Rev. B*, 74(10):104303, 2006.
 - [25] L. J. Rogers, S. Armstrong, M. J. Sellars, and N. B. Manson. Infrared emission of the NV centre in diamond: Zeeman and uniaxial stress studies. *New Journal of Physics*, 10(10):103024, 2008.
 - [26] Lachlan Rogers. How far into the infrared can a colour centre in diamond emit? *Physics Procedia*, 3(4):1557–1561, February 2010.
 - [27] J. P. Goss, R. Jones, S. J. Breuer, P. R. Briddon, and S. Öberg. The twelve-line 1.682 eV luminescence center in diamond and the vacancy-silicon complex. *Physical Review Letters*, 77(14):3041–3044, September 1996.
 - [28] N.B. Manson and R.L. McMurtrie. Issues concerning the nitrogen-vacancy center in diamond. *Journal of Luminescence*, 127(1):98–103, November 2007.
 - [29] Adam Gali, Maria Fyta, and Efthimios Kaxiras. Ab initio supercell calculations on nitrogen-vacancy center in diamond: Electronic structure and hyperfine tensors. *Phys. Rev. B*, 77:155206, 2008.
 - [30] Paul Delaney, James C. Greer, and J. Andreas Larsson. Spin-polarization mechanisms of the nitrogen-vacancy center in diamond. *Nano Letters*, 10(2):610–614, February 2010.
 - [31] A A Kaplyanskii. Noncubic centers in cubic crystals and their piezospectroscopic investigation. *Opt. Spectrosc.*, 16:329–337, 1964.
 - [32] A A Kaplyanskii. Computation of deformation splitting of spectral transitions in cubic crystals. *Opt. Spectrosc.*, 16:557–565, 1964.
 - [33] A E Hughes and W A Runciman. Uniaxial stress splitting of doubly degenerate states of tetragonal and trigonal centres in cubic crystals. *Proc. Phys. Soc.*, 90:827–838, 1967.
 - [34] P.A. Crowther and P.J. Dean. Phonon interactions, piezo-optical properties and the inter-relationship of the n3 and n9 absorption-emission systems in diamond. *Journal of Physics and Chemistry of Solids*, 28(7):1115–1136, July 1967.
 - [35] Gordon Davies. Dynamic jahn-teller distortions at trigonal optical centres in diamond. *J. Phys. C*, 12(13):2551–2566, 1979.
 - [36] Neil Manson, Lachlan Rogers, Marcus Doherty, and Lloyd Hollenberg. Optically induced spin polarisation of the NV- centre in diamond: role of electron-vibration interaction. arXiv e-print 1011.2840, November 2010.
 - [37] M W Doherty, N B Manson, P Delaney, and L C L Hollenberg. The negatively charged nitrogen-vacancy centre in diamond: the electronic solution. *New Journal of Physics*, 13(2):025019, February 2011.
 - [38] J R Maze, A Gali, E Togan, Y Chu, A Trifonov, E Kaxiras, and M D Lukin. Properties of nitrogen-vacancy centers in diamond: the group theoretic approach. *New Journal of Physics*, 13(2):025025, February 2011.
 - [39] Frank S Ham. Jahn-teller effects in electron paramagnetic resonance spectra. In S. Geschwind,

- editor, *Electron Paramagnetic Resonance*, pages 1–119. Plenum Press, 1972.
- [40] C. A Coulson and Mary J Kearsley. Colour centres in irradiated diamonds. i. *Proceedings of the Royal Society of London. Series A. Mathematical and Physical Sciences*, 241(1227):433–454, September 1957.
- [41] A. Lenef and S. C Rand. Electronic structure of the n-v center in diamond: Theory. *Phys. Rev. B*, 53(20):13441–13455, May 1996.
- [42] N. B. Manson, K. Beha, A. Batalov, L. J. Rogers, M. W. Doherty, R. Bratschitsch, and A. Leitenstorfer. Assignment of the NV^0 575-nm zero-phonon line in diamond to a e^-a_2 transition. *Physical Review B*, 87(15):155209, April 2013.
- [43] R. Jones, J. P. Goss, P. R. Briddon, and S. Öberg. N_2 and N_4 optical transitions in diamond: A breakdown of the vacancy model. *Physical Review B*, 56(4):R1654–R1656, July 1997.